

СИБИРСКИЕ ЭЛЕКТРОННЫЕ  
МАТЕМАТИЧЕСКИЕ ИЗВЕСТИЯ

Siberian Electronic Mathematical Reports

<http://semr.math.nsc.ru>

---

*Том 11, стр. 532–547 (2014)*

УДК 550.344.42, 519.633.2

MSC 76B15, 35L40, 65F22

SOME PROPERTIES OF THE INVERSE OPERATOR FOR  
A TSUNAMI SOURCE RECOVERY

T.A. VORONINA, V.A. TCHEVERDA, V.V. VORONIN

ABSTRACT. The application of an inversion method to the problem of recovering the initial water elevation field generating a tsunami is considered. This article addresses the usually ill-posed problem of the hydrodynamical inversion of remote measurements of water-level data without any a priori information on a source but its very general spatial localization. The tsunami wave propagation is considered within the scope of the linear shallow-water theory. The ill-posed inverse problem at hand is regularized by means of the least square inversion using the truncated *SVD* approach. Some properties of inverting operator in the context of retrieving a tsunami source are studied numerically. The goodness of the inversion is defined by the relative errors of the tsunami source reconstruction. As the result, we find the dependence of the goodness of the inversion in terms of the number of receivers, their azimuthal coverage and the frequency band. The applied approach allows one to control the instability of the numerical solution and to obtain an acceptable result in spite of the ill-posedness of the problem and makes it possible to predict a probable quality of the inversion by a certain observational system. This result should be kept in mind when designing a tide-gauge network to study a tsunami source.

**Keywords:** numerical modeling, tsunamis, regularization, singular value decomposition, *r*-solution, ill-posed inverse problem.

---

VORONINA T.A., TCHEVERDA V.A., VORONIN V.V., SOME PROPERTIES OF THE INVERSE OPERATOR FOR A TSUNAMI SOURCE RECOVERY.

© 2014 VORONINA T.A., TCHEVERDA V.A., VORONIN V.V.

The research was supported by Russian Foundation for Basic Research grants no. No 12-07-00406, by the Siberian Branch of the RAS (Project 117) and the Far-East Branch of the RAS (Project 37).

*Received May, 26, 2014, published June, 3, 2014.*

## 1. INTRODUCTION

This paper outlines some aspects of an approach to reconstructing an initial water elevation field that generates a tsunami. Recently, the devastating tsunamis have acutely put forward the problem for their timely warning and, as consequence, the importance of the accurate tsunami simulation. Mathematical modeling of tsunamis is to provide tsunami-withstanding communities with reliable information of inundation heights and arrival times for the purpose to immediate protective measures. Numerical modeling of a tsunami source is an important tool of assessment and mitigation of the negative effects of tsunamis.

Among mathematical approaches based on the inversion of near-field water-level data, most often used are the methods relying upon Green's functions technique (GFT) [1], the least square inversion combined with the GFT [3] or an optimization approach [2]. These methodologies with various modifications are widely used in practice. Later, the method proposed by V.Titov in [4] for refining source coefficient estimates based on seismic information by making use of data from Deep-ocean Assessment and Reporting of Tsunamis (*DART<sup>R</sup>*) buoys. The method involves using these data to adjust precomputed models via an inversion algorithm so that residuals between the adjusted models and the *DART<sup>R</sup>* data are as small as possible in a least squares sense.

This paper deals with an application of an original approach to the problem of retrieving the initial water elevation field (*tsunami source*) based on the inversion of remote measurements of water-level data (*marigrams*). This inversion method was first proposed by T.A.Voronina and V.A.Tcheverda in 1998 [5] and was already described in its fundamentals in previous papers [6], [7], [8]. Particularly, the proof of the compactness of the inverse problem operator was first presented for an arbitrary shape of bottom in [6]. In this method, the data space consists of a given number of tide-gauge records, and the model parameter space is represented by the values of the initial water elevation field at a given number of points.

The direct problem of the tsunami wave propagation is considered within the scope of the linear shallow-water theory. The ill-posed inverse problem of reconstructing initial tsunami waveforms is regularized by means of the least-square inversion using the truncated SVD approach. As a result of the numerical process, an *r*-solution is obtained [11]. In the present paper, the properties of inverting operator are studied by means of numerical modeling. This study is aimed at investigation of the characteristics of the method avoiding the influence of such a factor as bathymetry and deals, particularly, with establishing the dependence of the goodness of the inversion on the number of receivers, their azimuthal coverage and the frequency band when the computational domain is a right-angle basin. The method presented allows one to control the instability of the numerical solution and to obtain an acceptable result in spite of the ill-posedness of the problem.

## 2. MODELS

Mathematically, the problem of reconstructing the initial tsunami waveform in the source area is formulated as determination of spatial distribution of an oscillation source using remote measurements on a finite set of points (later called as *receivers*). Let us consider the coordinate system *xyz* and direct the axis-*z* downwards. The plane  $\{z = 0\}$  corresponds to the undisturbed water surface. The spherical shape of the Earth is neglected. Consider the aquatic part  $\Phi$  of a rectangular domain  $\Pi = \{(x; y) : 0 \leq x \leq X; 0 \leq y \leq Y\}$  on the plane  $\{z = 0\}$  with the solid boundaries  $\Gamma$  and the open sea boundaries. The arrival of the wave on the coast is not considered in this study. One of the main advantages of this method is that it is completely independent of any particular source model. Let  $\Omega = \{(x, y) : x_1 \leq x \leq x_M; y_1 \leq y \leq y_N\}$  be a tsunami source subdomain of  $\Phi$ . The observational data are the water level records which are assumed

to be known at a set of points in the domain  $\Phi$ . Since a tsunami in the ocean is a long gravitational wave with a low amplitude, its propagation can be considered in the scope of the linear shallow water theory. Let  $\eta(x, y, t)$  be a function of the water surface elevation relative to the mean sea level which is considered to be a solution of the linear shallow water equation:

$$(1) \quad \eta_{tt} = \operatorname{div}(gh(x, y)\operatorname{grad}\eta) + f_{tt}(x, y, t)$$

with the initial conditions:

$$(2) \quad \eta|_{t=0} = 0; \quad \eta_t|_{t=0} = 0$$

completed on the continental coasts with zero Neumann boundary conditions:

$$(3) \quad \left. \frac{\partial \eta}{\partial n} \right|_{\Gamma} = 0,$$

and the boundary conditions simulated on an open boundary when the spatial boundary occurs in an ocean location. The second order absorbing boundary conditions were used at the open boundaries [9]. The tsunami wave is assumed to be triggered by a sudden vertical displacement  $f(x, y, t)$  of the sea floor. It is assumed that

$$(4) \quad f(x, y, t) = H(t)\varphi(x, y),$$

where  $\varphi(x, y)$  is a co-seismic vertical displacement and  $H(t)$  is the Heaviside step function. As a result  $\varphi(x, y)$  is the initial sea surface deformation in the target domain  $\Omega$ . The acceleration of gravity is the constant  $g$  and the wave phase velocity is defined as  $c(x, y) = \sqrt{gh}$ . In addition, the function  $\eta(x, y, t)$  is assumed to be known at a set of points  $M = \{(x_i, y_i), i = 1, \dots, P\}$

Let us consider a special case for the approach proposed when the computational domain is the parallelepiped with the height  $h_0$  based on the rectangular  $\Pi$ , the wave phase velocity is defined as  $c(x, y) = c_0 = \sqrt{gh_0}$ , boundary condition (2) being correct for the line  $y = 0$  and the free boundary condition corresponding to the lines  $\{x = 0; y = Y; x = X; \}$  in the plane  $\{z = 0\}$ . With these assumptions, equation (1) can be rewritten in the form:

$$(5) \quad \frac{1}{c_0^2}\eta_{tt} = \Delta\eta + \frac{1}{c_0^2}f_{tt}(t, x, y).$$

This makes possible to consider the analytical solution of the above equation in the spectral domain. Let us denote:

$$(6) \quad \bar{\eta}(x, y; \omega) = \int_{-\infty}^{\infty} \eta(x, y, t)e^{-i\omega t} dt$$

$$(7) \quad \bar{f}(\omega, x, y) = \int_{-\infty}^{\infty} f(x, y, t)e^{-i\omega t} dt,$$

where function  $f(x, y, t)$  is defined by (4). After applying the Fourier transform with respect to time, one can obtain the following inverse problem: to recover the function  $\varphi(x, y) \in L_2(\Omega)$  with a known spectrum of the function  $\bar{\eta}(x, y; \omega)$  for a certain frequency band  $[\omega_1, \omega_2]$

$$(8) \quad \bar{\eta}(x, y; \omega)|_M = \bar{\eta}_o(x_j, y_j, \omega); \quad \omega_1 \leq \omega \leq \omega_2$$

with  $\bar{\eta}(x, y; \omega)$  being the solution to the Helmholtz equation

$$(9) \quad \Delta\bar{\eta} + \frac{\omega^2}{h_0}\bar{\eta} = \frac{i\omega}{c_0}\varphi(x, y)$$

satisfying the Sommerfeld radiation condition. Therefore, the recorded field depends on the source amplitude in the following manner:

$$(10) \quad \bar{\eta}_0(x, y, \omega) = \frac{-i\omega}{c_0^2} \iint_{\Omega} \varphi(\xi, \zeta) H_0^{(1)} \left( k \sqrt{(x - \xi)^2 + (y - \zeta)^2} \right) d\xi d\zeta, \\ i = 1, \dots, P,$$

where  $k \equiv \omega/c_0$ , and  $H_0^{(1)} \left( k \sqrt{(x - \xi)^2 + (y - \zeta)^2} \right)$  is Hankel's function. Let us denote  $F(\omega) = -i\omega/c_0^2$ . For the data space, let us consider that the observational system consists of  $P$  receivers disposed at a set of points  $\{(x_i, y_i), i = 1, \dots, P\}$ , where the spectrum of the recorded field  $\bar{\eta}_0(x, y, \omega_j)$  is known for some frequency setting  $\{\omega_j\} j = 1, \dots, K_\omega$ . In order to obtain a system of linear algebraic equations by means of a projective method, a trigonometric basis was chosen in the model space, i.e., the unknown function  $\varphi(x, y)$  was sought for as a series of spatial harmonics  $\{\varphi_{mn}(x, y) = \sin \frac{m\pi}{l_1}(x - x_1) \cdot \sin \frac{n\pi}{l_2}(y - y_1), m = 1, 2, \dots, M; n = 1, 2, \dots, N\}$  and the center of the tsunami source was believed to be at the point  $(x_c, y_c)$ , being the central point of the domain  $\Omega$ . Here  $l_1 = (x_M - x_1); l_2 = (y_N - y_1)$ . Thus, the unknown function of water surface elevation  $\varphi(x, y)$  is approximated by the sum of spatial harmonics:

$$(11) \quad \varphi(x, y) = \sum_{m=1}^M \sum_{n=1}^N c_{mn} \sin \frac{m\pi}{l_1}(x - x_1) \cdot \sin \frac{n\pi}{l_2}(y - y_1)$$

with unknown coefficients  $\{c_{mn}\}$  in the domain  $\Omega$ . This leads to the following system of linear algebraic equations with respect to the coefficients  $c_{mn}$  according to formula (11):

$$(12) \quad \bar{\eta}_0(x_i, y_i, \omega_j) = F(\omega_j) \sum_{m=1}^M \sum_{n=1}^N c_{mn} \int_{x_1}^{x_M} \int_{y_1}^{y_N} \sin \frac{m\pi}{l_1}(\xi - x_1) \sin \frac{n\pi}{l_2}(\zeta - y_1) \times \\ \times H_0^{(1)} \left( k_j \sqrt{(x_i - \xi)^2 + (y_i - \zeta)^2} \right) d\xi d\zeta$$

In order to compute these integrals, the uniform grid was introduced over the rectangle  $\Omega$  with the parameters  $I, Q$  over  $x$ - and  $y$ - directions, respectively:  $h_x = l_1/I, h_y = l_2/Q, \xi_p = h_x \cdot p; p = 0, \dots, I, \zeta_q = h_y \cdot q; q = 0, \dots, Q$ . Within each elementary rectangle  $[\xi_i \leq \xi \leq \xi_i + h_x] \times [\zeta_q \leq \zeta \leq \zeta_q + h_y]$  a bilinear approximation denoted as  $\tilde{H}_{iq}(\xi, \zeta)$  for Hankel's function was used. Let us denote  $H_{i,j,p,q} = H_0^{(1)} \left( k_j \sqrt{(x_i - \xi_p)^2 + (y_j - \zeta_q)^2} \right), \bar{\eta}_{0,i,j} = \bar{\eta}_0(x_i, y_i, \omega_j)$ . Then system (12) could be rewritten in the form

$$(13) \quad \bar{\eta}_{0,i,j} = F_j \sum_{m=1}^M \sum_{n=1}^N c_{mn} \sum_{p=1}^{I-1} \sum_{q=1}^{Q-1} \int_{\xi_p}^{\xi_p+h_x} \int_{\zeta_q}^{\zeta_q+h_y} \sin \frac{m\pi}{l_1}(\xi - x_1) \sin \frac{n\pi}{l_2}(\zeta - y_1) \times \\ \times \tilde{H}_{pq}(\xi, \zeta) d\xi d\zeta.$$

There is another fact to be remarked: the function  $\bar{\eta}_0(x, y, \omega_j)$  is a complex one when the unknown function  $\varphi(x, y)$  describing the source amplitudes is a real one. Therefore, the unknown coefficients  $\{c_{mn}\}$  will be real, too. This fact was taken into account in the algorithm and by standard technique a new system with only real equations was obtained from system (13). Thus, the number of equations in new system will be equal to  $L = 2 \times P \times K_\omega$ .

Now, it is possible to use the **r**-solution method for system (13) as it will be explained below.

### 3. INVERSION METHOD

The proposed inversion method was described in details in previous papers [6], [7], [8] for the continuous case. In this case, let us denote by  $A$  the linear operator of the Cauchy problem (1)-(3), which is defined in the following way: for each given  $\varphi(x, y)$

solve the problem (1)-(3) and trace its solution on the line  $\gamma$  (a smooth curve without self-intersection):

$$(14) \quad A < \varphi > = \eta_0(s, t),$$

where

$$\eta_0(s, t) = \eta(x(s), y(s), t), \quad (x(s), y(s)) \in \gamma(s), \\ 0 \leq t \leq T, \quad 0 \leq s \leq L$$

The inverse problem in question can now be formulated as a problem of solving the linear operator equation of the first kind. As was shown by A.Kaistrenko in [10], the above inverse problem has a unique solution only if the source function allows factorization with the time and spatial variables.

Its solution will be sought for in the least squares formulation. The operator  $A : L_2(\Omega) \rightarrow L_2(\gamma(s) \times (0, T))$  is a compact one because its kernel is a function with weak singularity and, therefore, this operator does not possess a bounded inverse. In other words, any attempt to numerically solve equation (14) must be followed by a certain regularization procedure. In the present paper, regularization is performed by means of the truncated *SVD* that brings about the a notion of **r**-solution (see [11]).

In brief, the notion of **r**-solution can be described as follows. Any compact operator  $A$  could be described in the Hilbert spaces with the singular system  $\{s_j, \vec{u}_j, \vec{v}_j\}, j = 1, \dots, \infty$ , where  $s_j \geq 0$  ( $s_1 \geq s_2 \geq \dots \geq s_j \geq \dots$ ) are singular values and  $\{\vec{u}_j\}, \{\vec{v}_j\}$  are the left and the right singular vectors.  $A\vec{v}_j = s_j\vec{u}_j$  and  $s_j \rightarrow 0$  with  $j \rightarrow \infty$ . The systems  $\{\vec{u}_j\}, \{\vec{v}_j\}$  are orthogonal. A very important property of the singular vectors is that they form bases in the data and model spaces and the solution of equation (14) can be given by expression

$$(15) \quad \varphi(x, y) = \sum_{j=1}^{\infty} \frac{(\eta_0(s, t) \cdot \vec{u}_j)}{s_j} \vec{v}_j(x, y).$$

The solution given by (15) is nothing else as the "normal general" solution and operator, given by the right-hand side of (15) is normal general pseudoinverse for  $A$  ([12]). As one can see from formula (15) the ill-posedness of the operator equation of the first kind with the compact operator is due to the fact that  $s_j \rightarrow 0$  with  $j \rightarrow \infty$ , i.e. one can perturb the right-hand side  $\eta_0(s, t)$  in such a way, that its vanishing perturbation  $\varepsilon(t)$  can lead to a large perturbation of the solution.

The regularization procedure based on truncated *SVD* leads to the notion of **r**-solution given by the relation:

$$(16) \quad \varphi^{[r]}(x, y) = \sum_{j=1}^r \frac{(\eta_0(s, t) \cdot \vec{u}_j)}{s_j} \vec{v}_j(x, y).$$

The **r**-solution is the projection of the exact solution (15) onto a linear span of the **r** right singular vectors corresponding to the top singular values of the compact operator  $A$ . This truncated series is stable for any fixed parameter **r** with respect to perturbations of right-hand side and operator itself ([11]). It is reasonable that the larger **r**, the more informative is the solution obtained. Finally, the value of **r** is determined by the singular spectrum of the matrix **A** which is tightly bounded with the parameters of the observation system.

#### 4. NUMERICAL EXPERIMENTS: DESCRIPTION AND DISCUSSION

A series of calculations were carried out by the method proposed to set up the dependence of the goodness of an inverted function on certain characteristics of the observational system such as the number and location of receivers, the frequency band of the data. As the main objective of our research is an application to reconstructing an initial tsunami waveform, we can assume the location of the target domain  $\Omega$  to be known. In the truly real cases, the tsunami source area is specified from seismological data shortly after the event. Synthetic data for the numerical inversion experiments presented below

were computed as a solution of problem (1) - (2) with appropriate boundary conditions and a function  $\varphi(x, y)$  in the form

$$(17) \quad \varphi(x, y) = \beta(x, y) \cdot \alpha(x),$$

where the parameter  $\alpha(x)$  was selected according to the case study that will be clear in what follows. Let us introduce the notation

$$\mathbf{Pa}(x, y) = \frac{(x - x_0)^2}{R_1^2} + \frac{(y - y_0)^2}{R_2^2},$$

then the function  $\beta(x, y)$  describes a semi-paraboloid:

$$(18) \quad \beta(x, y) = \begin{cases} 1 - \frac{(x-x_0)^2}{R_1^2} - \frac{(y-y_0)^2}{R_2^2} & , \text{ if } \mathbf{Pa}(x, y) < 1 \\ 0 & , \text{ if } \mathbf{Pa}(x, y) \geq 1. \end{cases}$$

The numerical simulation includes the following steps:

1) First, we obtain the synthetic *marigrams* in all receivers by solving the forward problem with appropriate boundary conditions and a certain function  $\varphi(x, y)$  as a source which to be reconstructed. Thus, the vector  $\bar{\eta}_0(x, y, w)$  in (12) is obtained.

2) Next, the matrix  $\mathbf{A}$  is numerically computed by solving the forward problem with every spatial harmonic  $\varphi_{mn}(x, y) = \sin \frac{m\pi}{l_1}x \cdot \sin \frac{n\pi}{l_2}y$ ,  $m = 1, \dots, M; n = 1, \dots, N$  as initial condition.

3) Further, standard SVD- procedure is applied. The analysis of singular spectrum of the matrix  $\mathbf{A}$  allows one to define the number  $\mathbf{r}$  and to compute the coefficients  $\{c_{mn}\}$  as an  $\mathbf{r}$ -solution by (12).

4) After this, the function  $\hat{\varphi}(x, y)$  can be computed in the form (11).

6) Finally, to estimate the goodness of an inversion experiment we use an  $l_2$ -norm misfit parameter that represents the squared averaged difference between the exact solution function  $\{\varphi_i = \varphi(x_i, y_i)\}$  and the recovered one  $\{\hat{\varphi}_i = \hat{\varphi}(x_i, y_i)\}$ :

$$err\% = \left( \frac{\sum_{i=1}^K (\varphi_i - \hat{\varphi}_i)^2}{\sum_{i=1}^K (\varphi_i)^2} \right)^{1/2} \times 100\%,$$

where  $i = n + (m - 1) \times N; n = 1, \dots, N; m = 1, \dots, M; K = N \times M$ .

A series of the calculations were made by the method proposed and were aimed at recovering the unknown function  $\varphi(x, y)$  in the form (11). Let us assume: a flat bathymetry  $h(x, y) = 4.082$  ( below all distances are scaled in kilometers); the wave velocity  $c_0 = const = 0.2 km/sec$ ;  $\alpha(x) = 1$  in formula (17), i.e. the initial field is only a turning-up function. Let us denote a computational domain on surface  $\{z = 0\}$  as a rectangle  $\Pi = \{(x; y) : -X \leq x \leq X; 0 \leq y \leq Y\}$  encompassing all the receivers and the source area  $\Omega$ . We assume that the total reflective boundary condition (3) was fulfilled on the line  $y = 0$  and an open boundary corresponded to the lines  $x = 0; x = X; y = Y$ . The center of the source was located at  $(x_0, y_0) = (0, 150)$ . The function  $\varphi(x, y)$  was sought for according to formula (11) with  $M = 21, N = 21$ , its maximum value being  $\varphi_{max} = 1 m$ , and the domain  $\Omega$  was a spatial discretization by means of  $100 \times 100$  mesh points, i.e.  $I = 101$  and  $Q = 101$  in (13).

Let us define an assembly of the above specifying parameters as *Pattern 1* and designate as *Model (Mod.)* the total sum of the *Pattern 1* and additional parameters such as  $K_p$  - the number of receivers,  $K_w$  - the number of frequencies and the range of frequency band and geometry of aperture. Over this all computation were made for the four values of conditions number of the matrix  $A$ :  $10^2; 10^4; 10^6; 10^8$ . All following graphs of singular spectra of the matrix  $A$  are in the common logarithm scale.

We introduce the following notations:

- (1) the words "the conditioning number of the matrix  $A$  were designated as  $cond(A)$ ;
- (2) the value  $100 \times max(\varphi(x, y))$ , while  $(x, y) \in \Omega$  is denoted by the symbol  $\{100max\}$ ;

(3) the misfit parameter is denoted by  $\text{err}\%$ .

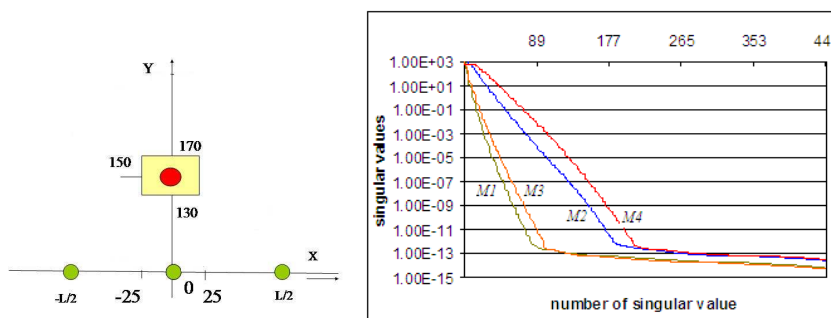


FIG. 1. The source-receivers arrangement: the source (red circle), the target domain  $\Omega$  (yellow rectangle), the receivers (green circles) (left). The singular spectra of the matrix  $A$  (common logarithm scaled) in *Models* 1,2,3,4 with the numbers of their singular values (right).

Figure 1(left) shows the layout scheme of the source-receivers arrangement for *Models* 1 – 4. The spatial parameters of the source were specified by the following way: a half-sphere with a radius  $R_s = 5$ ;  $\Omega = \{(x, y) : -25 \leq x \leq 25; 130 \leq y \leq 170\}$ . In the inversion by *Models* 1 – 4, the following values of the parameters were used:  $K_p = 11, K_w = 50, A = (1100 \times 441)$ . In these *Models* the receivers are uniformly distributed along the line  $y = 0$  as much as possible along the interval  $[-L/2, L/2]$ :

$$\text{Model1} : w \in [0.0005, 0.002] \text{Hz}; L = 100;$$

$$\text{Model2} : w \in [0.002, 0.01] \text{Hz}; L = 100;$$

$$\text{Model3} : w \in [0.0005, 0.002] \text{Hz}; L = 1000;$$

$$\text{Model4} : w \in [0.002, 0.01] \text{Hz}; L = 1000;$$

These inversion experiments were carried out to answer the question how the goodness of the inversion depends on the aperture length and the frequency band. First of all, we analyzed the singular spectrum of the matrix  $A$  for *Models* 1–4. In Figs.1-3 the correlation between *Models* and color of lines is following: *Mod.1* (green); *Mod.2* (blue); *Mod.3* (orange) and *Mod.4* (red). The common logarithm of the singular values were plotted in Fig. 1(right). A sharp decrease in the singular values, when their number increases, is typical for all calculations in all cases of the study, due to the ill-posedness of the problem. Setting the parameter  $r$  is caused by a rapid decrease in the singular values of the matrix  $A$ . Fig.2 (left) shows the range of the number  $r$  becoming wider when the conditioning number of the matrix  $A$  is increasing. A larger  $r$  results in a more informative solution obtained: a maximum of the unknown function is increasing (Fig.2 (right)) and the misfit parameter ( $\text{err}\%$ ) is decreasing as one can see in Fig.3 (left). By analyzing the graphs in Fig.1 (right) we can expect the most successful outcome of the inversion process for the *Mod.4* (marked by the red color) because of a gently sloping curve of the singular spectrum that leads to increasing the number  $r$  used in the inversion. Comparing these values for different models one can see that the inversion becomes better while the aperture length becomes wider (compare the green and the orange lines corresponding to *Mod1* and *Mod3* and the blue and the red lines corresponding to *Mod2* and *Mod4*, respectively). These graphs show that increasing the upper limit of the frequency range makes the most effect for the inversion quality in the case studied (compare the green and the blue lines corresponding to *Mod1* and *Mod2* and the orange and the red lines corresponding to *Mod3* and *Mod4*, respectively). The diagrams in Fig.3 (right) confirm

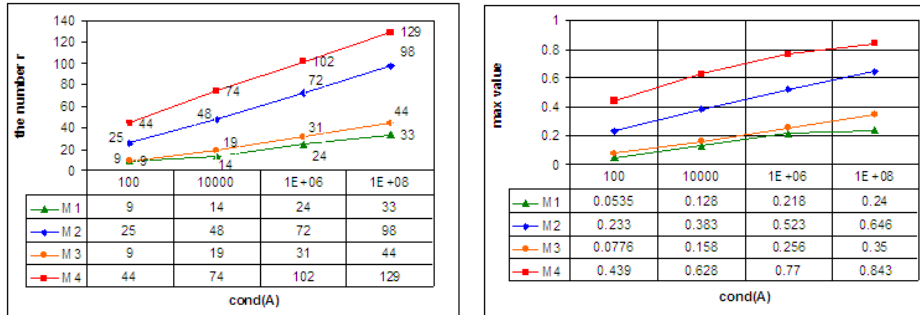


FIG. 2. The number  $r$  with the conditioning number of the matrix  $A$  in *Models* 1,2,3,4 (left). The largest extremum of the inverted function  $\hat{\varphi}(x, y)$  in terms of the conditioning number of the matrix  $A$  (*Models* 1-4) (right).

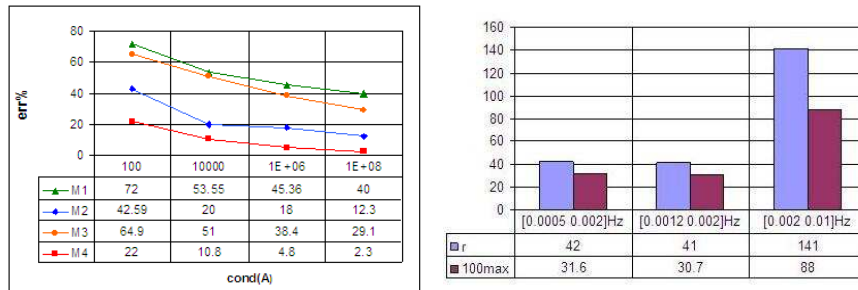


FIG. 3. The misfit parameter  $err\%$  in terms of the conditioning number of the matrix  $A$  (*Models* 1-4) (left). The diagrams of changing the inversion parameters with the upper limit of the frequency band when 10 receivers are uniformly distributed along the aperture line  $y = 0$ ;  $L = 1000$ ; and  $K_w = 20$  (right).

this conclusion. The functions inverted by the *Mods.* 1,2,3,4 ( $cond(A) = 10^8$ ) are presented in Fig.4. Figs.4(middle left) and (right) illustrate that an increase in the upper limit of

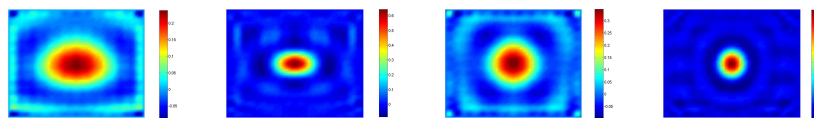


FIG. 4. The inverted functions by *Models* 1,2,3,4:  $L=100$ ; [0.0005,0.002]Hz (left);  $L=100$ ; [0.002,0.01]Hz (middle left);  $L=1000$ ; [0.0005,0.002]Hz (middle right);  $L=1000$ ; [0.002,0.01]Hz (right)

the frequency band leads to decreasing the "smearing" of the inverted function and, hence, to increasing a maximum value in the center of the source supposed.

In the second series of the inversion we studied the dependence of the inverted function on the geometry of the aperture. The computer simulations were made within the scope of *Patten 1* with the frequency band  $[0.0005, 0.002]Hz$ ;  $K_p = 11$ ;  $K_w = 50$  and the condition number  $cond(A) = 10^8$ . First, let us consider models when the receivers were distributed on the two sides of the angle  $BADC$  (see Fig.5) (left). In *Mod. 5.1* and *Mod. 5.2* five

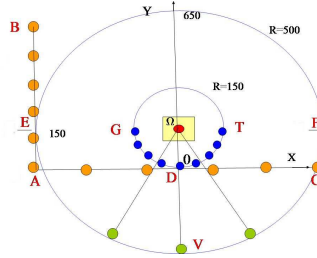


FIG. 5. The source-receivers arrangement for *Models 5-6*: the source (red circle), the target domain  $\Omega$  (yellow rectangle); the receivers (small circles on the lines  $BA$ ,  $AC$ , and on the segments of the circles  $EVF$  and  $GDT$ , respectively) (left).

receivers are distributed on the line  $BA$ ;  $B(-500, 600)$ ,  $A(-500, 0)$  with the interval 100 and the next six receivers are uniformly distributed on the lines  $AD$  or  $ADC$ , respectively. In other words, *Mod. 5.1* and *Mod. 5.2* are differed from each other by the aperture angle.

The influence of the receivers-to-source distance on the goodness of the inversion was investigated in *Mod. 6.1* and *Mod. 6.2* when all receivers are uniformly distributed on the semi-circles centered at the point  $(x_0, y_0) = (0, 150)$  with  $R = 150$  in *Mod. 6.1* and with  $R = 500$  in *Mod. 6.2* (the segments  $GDT$  and  $EVF$  of the circles in Figure 5) (left). In addition, we have carried out modeling when the frequency band was equal to  $[0.002, 0.01]Hz$  for the last cases named *Mod. 6.12* and *Mod. 6.22*, respectively.

The comparison of the singular spectra of all these *Models* plotted in Fig. 5 (right) allows one to estimate the goodness of the inversion for every *Model*. A most shape

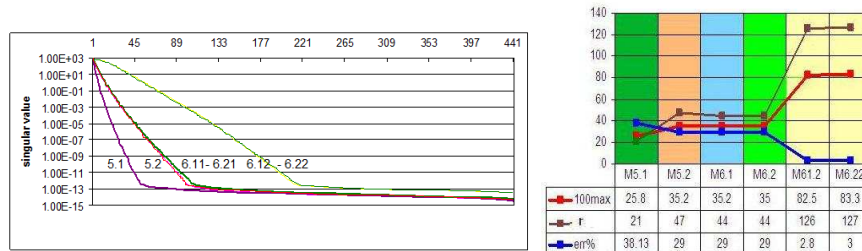


FIG. 6. The singular spectra of the matrix  $A$  for *Models*: 5.1 (magenta line), 5.2 (red line), 6.1 (blue line), 6.2 (green line), 6.12 (yellow line), 6.22 (light green line) (right). The number  $r$ , the misfit parameter  $err\%$  and the maximum value of  $\hat{\varphi}(x, y)$  in terms of *Mods.* 5.1, 5.2, 6.1, 6.2, 6.12, 6.22

decreasing in singular values of the singular spectrum of *Mod. 5.1* leads to a poor choice of the number  $r$  and, as consequence, to the unsuccessful version of the inversion. As is shown in Fig.6 (left), there are very similar singular spectra in *Models 5.2, 6.1, 6.2*. We can

expect that the inverted fields to be similar in shape, too. This fact is confirmed in Fig.7. A good similarity is observed between the singular spectra of *Mod.* 6.1 and 6.2 as well as between of *Mod.* 6.12 and *Mod.* 6.22. This makes possible to bring into coincidence in the number  $r$  for earth pair cases (see Fig.6 (right)) and, finally, it makes possible to obtain the coincidence of the inversion results. Furthermore, from the preceding arguments we can expect that the inversion results in *Models* 6.12 and 6.22 will be better than in *Models* 6.1 and 6.2, respectively. By analyzing plots in Fig.7 one can conclude:

(1) the results of the inversion by a wide angle aperture in *Mod.* 5.2 coincide with the experiments on the wide linear aperture  $L = 1000$  in *Mod.* 3. Indeed, a maximum value of the inverted function and misfit parameter are equal to  $\hat{\varphi}_{max} \approx 0.35$ ;  $err\% \approx 29\%$ .

(2) A receivers-to-source distance does not influence on the inversion result: compare the values in the blue and the green columns, corresponding to *Mod.* 6.1 and *Mod.* 6.2, respectively. They are qualitatively equivalent in the sense of maximum values of the inverted function, but their smearing is different (see Fig.7). After analyzing the plots in the blue, green and yellow columns in Fig.6 (left), we can conclude that an increase in the upper limits in the frequency band makes also the inversion better in these cases.

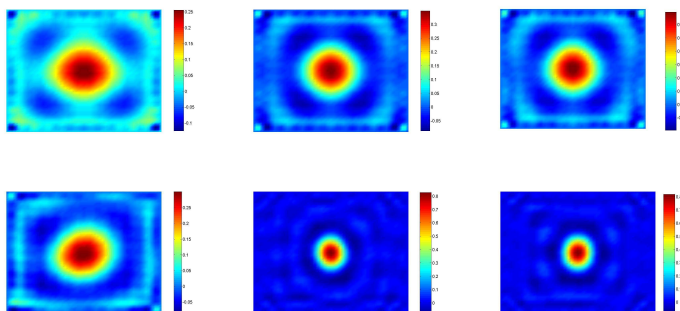


FIG. 7. The recovered functions: (top) by models *Mod.* 5.1 (left), *Mod.* 6.1 (middle) and *Mod.* 6.2 (right); (bottom) by models *Mod.* 5.2 (left), *Mod.* 6.12 (middle) and 6.22 (right).

**4.1. The dependence of the recovered function on the number of receivers and the aperture angle.** This issue is of primary practical importance: how goodness of the recovered function depends on the number of receivers used in the inversion procedure. First of all, our purpose was to obtain acceptable results of the inversion using a minimum number of marigrams. In this connection, we have made the computer simulation using a number of records that ranges from 1 to 30 with different azimuthal coverage.

Fig.8 shows the layout scheme of the source-receivers arrangement for *Models* 7 – 9. The target domain  $\Omega = \{(x, y) : -100 \leq x \leq 100; 100 \leq y \leq 200\}$ ,  $w \in [0, 001, 0, 01]Hz$ ;  $\alpha(x) = 1$  in relation (17) and  $cond(A) = 10^8$  in all calculations for these cases. It must be mentioned that the value  $K_w$  in the experiments performed was defined so that  $K_p \times K_w$  remains constant.

Let us consider *Mod.* 7 based on *Pattern* 1 with the linear aperture along the line  $y = 0$ ,  $L = 1000$  (according to Fig.8) and the number of receivers being: 3, 5, 8, 15, 20, 30. These receivers were uniformly distributed along the aperture. In *Table* 1 one can see the main characteristic of the *Models* 7-9 more particular.

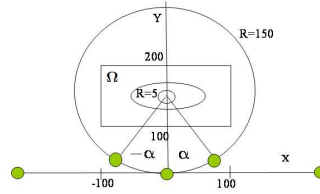


FIG. 8. The source-receivers arrangement on the surface  $z = 0$ : source for *Model 7* (central small circle); for *Model 8 – 9* (central ellipse); receivers (the green small circles)

Table1

Model	type of the aperture	number of the receivers	type of the source
Model 7	on the line $y=0$ ; $L=1000$	3,5,8,15,20,30	semi-sphere $R_1 = 5$ ; $R_2 = 5$
Model 8	on the line $y=0$ ; $L=200$	3,5,7,10,15	semi-ellipsoid $R_1 = 50$ ; $R_2 = 25$
Model 9	on the semi-circle $R=150$	1,2,3,5	semi-ellipsoid $R_1 = 50$ ; $R_2 = 25$

Let us consider *Mod.7* based on *Pattern 1* with the linear aperture along the line  $y = 0$ ,  $L = 1000$  (according to Fig.8) and the number of receivers being: 3, 5, 8, 15, 20, 30. These receivers were uniformly distributed along the aperture. Comparing the singular spectra for the *Mod.7* with different number of receivers in Fig.9 we can predict that the worse result will be in the inversion when 3 receivers were used, while the best result will be provided using 15-30 receivers. Indeed, in Fig.9 one can see how the number  $r$ , parameter  $K_w$  and a maximum value of the recovered function are changing with the number of receivers used in the inversion when  $cond(A) = 10^8$ . The goodness of

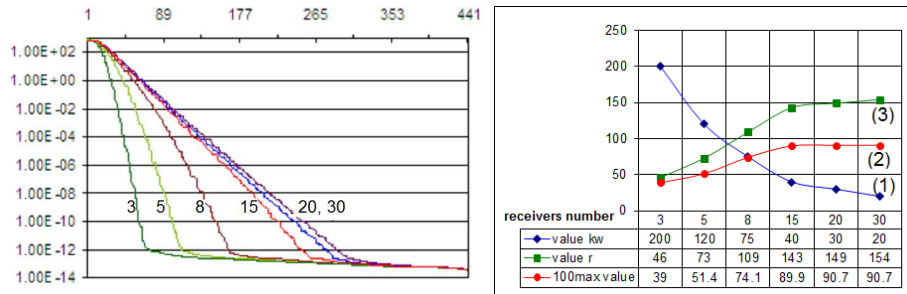


FIG. 9. The singular spectra of the matrix  $A$  for *Mod.7*; with a different numbers of receivers used in the inversion: 3(dark green), 5(light green), 8(violet), 15(red), 20(blue), 30(pink) (left). Dependence of the number  $r$ , a maximum value of the recovered function and the value  $K_w$  on the number of receivers in *Mod.7* (right).

the inversion is improving when the number of receivers increases up to 15. Obviously, further increasing is useless. This assumption is confirmed by the pictures of the recovered functions in Fig.10 (see maximum values of the recovered function in *Table* in Fig.9 (right)).

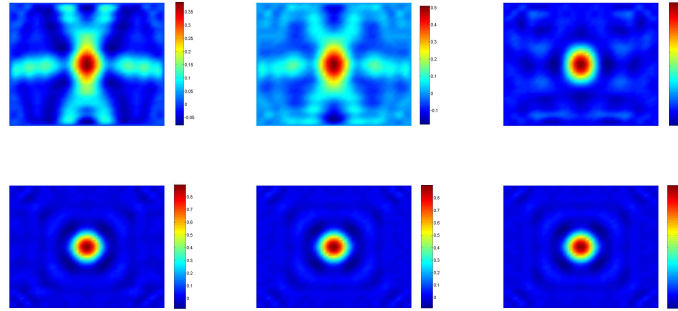


FIG. 10. The recovered functions in *Mod. 7* with: (top) 3 receivers (left); 5 receivers (middle); 8 receivers (right); (bottom) 15 receivers (left); 20 receivers (middle); 30 receivers (right).

Let us change some spatial parameters in our *Models*. Let now the function  $\varphi(x, y)$  be a semi-ellipsoid, while  $\alpha(x) = 1$ ;  $R_1 = 50$ ;  $R_2 = 25$  according to relations (17)-(18) and the number of receivers vary: from 3 to 15 in *Mod. 8* and from 1 to 5 in *Mod. 9*. In accordance with Figure 8, in *Mod. 8* receivers are uniformly distributed on the line

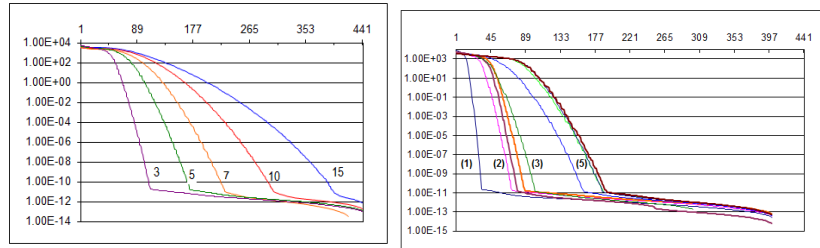


FIG. 11. The singular spectra of the matrix  $A$  in *Mod. 8* in terms of the number of receivers (left). The singular spectra of matrix  $A$  in *Mod. 9* for different receivers aperture angle: 1 receiver (the dark magenta line); 2 receivers and the aperture angles:  $\pi/5$  (the pink line);  $3\pi/5$  (the brown line);  $\pi$  (the orange line); 3 receivers  $\pi/5$  (the green line); 5 receivers with aperture angles:  $\pi/10$  (the blue line);  $\pi/2$  (the light green line);  $2\pi$  (the magenta line) right).

$y = 0$ ;  $L = 200$ , but in *Mod. 9* receivers were set on the segment  $[-\alpha, \alpha]$  of the circle centered at the point  $(0, 150)$  with  $R = 150$  and the aperture angle is equaled  $2\alpha$ , while  $\alpha = n \times \pi/10$ ;  $n = 0.5, 1, 2.5, 3, 5, 6, 10$ . In *Mod. 8* the number of frequencies was equal to 30 ( $K_w = 30$ ) for the inversion by 15, 10, 7 marigrams,  $K_w = 50$  for the case with 5 marigrams and  $K_w = 100$  for the case with 3 marigrams, respectively.

As is clear from Fig.11 the behavior of the singular spectra as a function of the number of receivers in *Mod. 8* and in *Mod. 9* keeps the main features being typical of the ill-posed problem singular spectrum. Increasing the number of receivers leads to moving the singular spectra in such a way that the available interval of the number  $\mathbf{r}$  is increasing and this results in obtaining a more informative solution, i.e. the inversions become more

robust. The latter is confirmed by the Fig.12 where the recovered functions by *Mod. 8* are represented.

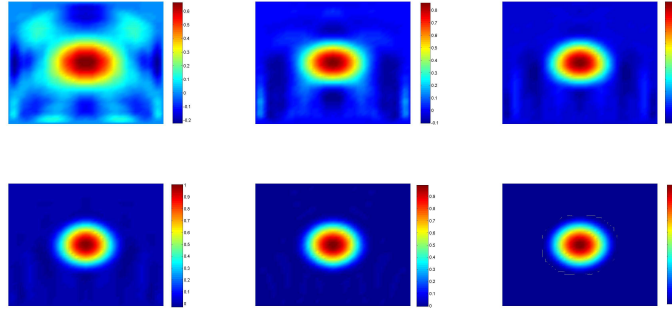


FIG. 12. The recovered functions in *Mod. 8* with: (top) 3 receivers (left); 5 receivers (middle); 7 receivers (right); (bottom) 10 receivers (left); 15 receivers (middle); the theoretical function  $\varphi(x, y)$  (right).

Next, we present the results obtained in *Mod. 9* when the goodness of the inversion was studied with a range of the aperture angle and the number of receivers.

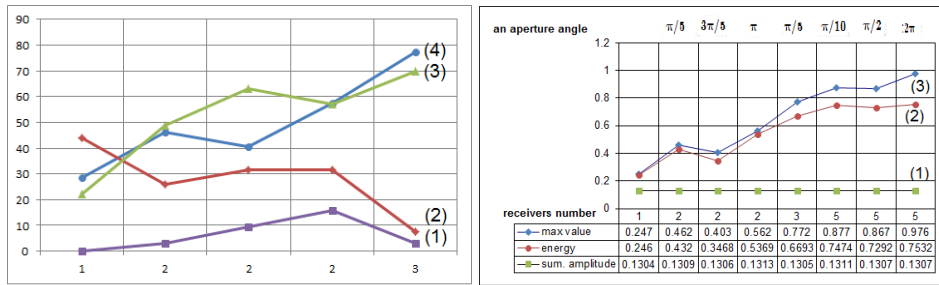


FIG. 13. The graphs of changing the inversion parameters with the number of used receivers in *Mod. 9*: half-aperture angle ( $\alpha$ ) multiplied by 10 (the line 1); the misfit parameter (the line 2); the number  $r$  (the line 3) and the maximum value multiplied by 100 (the line 4)(left). The diagram of changing the inversion parameters with the number of receivers used in the calculations in *Mod. 9* : displaced water volume multiplied by  $10^4$  (the line 1); released energy multiplied by  $10^3$  (the line 2) and the maximum value of the recovered function multiplied by 100 (the line 3) (right).

Adding new receivers in *Mod. 9* leads to increasing a maximum value of the recovered function from the value 0.28 to the value 0.876 (the line (3) in Fig.13 (left)) and, simultaneously, to decreasing the misfit parameter from 44% to 2.43% (the line (2) in Fig.13 (left)) for the cases with different aperture angles. One can see in Fig.13 (right) that the released energy is increasing as well as maximum value of inverted function, but the total displacement volume ("sum amplitude") as is not changes in our experiments.

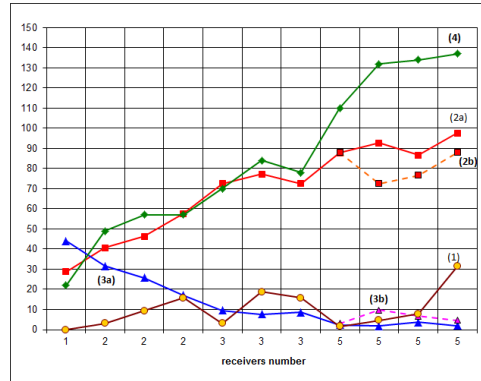


FIG. 14. The diagram of changing the inversion parameters with the aperture angle range and the number of receivers used in *Model 9*. There are solid lines: half-aperture angle multiplied by 10 (the line 1);  $cond(A) = 10^8, 100max$  (the line 2a) and the misfit parameter  $err\%$  (the line 3a); the number  $r$  (the line 4) and the dashed lines  $cond(A) = 100: 100max$  (the line 2b) and the misfit parameter  $err\%$  (the line 3b)

Let us discuss the graphs plotted in Fig.14. As is clear, increasing the number of receivers, in total, leads to the more robust inversion: the misfit parameter (the line 3a) is decreasing while maximum value (the line 2a) of the recovered function tends to maximum value (100) of the theoretical function. If the number of receivers is fixed the goodness of the inversion rises with the azimuthal coverage (the line 1). In addition, we studied the dependence of such inversion parameters as maximum value of the recovered function and the misfit parameter on the conditioning number of the matrix  $\mathbf{A}$ . In addition, when 5 receivers were used, the simulation was made with  $cond(\mathbf{A}) = 100$  (see 3b and 2b dashed lines in Fig.14). Comparing lines 3a and 2a with lines 3b and 2b, respectively, one can see that if the aperture angle (the line 1) is sufficiently wide, the influence of the conditioning number is not significant. The recovered functions for the above discussed cases are presented in Figs.15-16 (compare with the theoretical function for *Models 8, 9* in Fig.12 ( bottom right)). The best result was obtained when the source area is ringed by

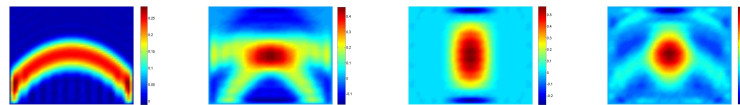


FIG. 15. The recovered functions in *Mod.9* by the inversion with: 1 receiver (left); 2 receivers;  $\alpha = 0.1\pi$  (middle left); 2 receivers;  $\alpha = 0.5\pi$  (middle right); 3 receivers;  $\alpha = 0.1\pi$  (right).

receivers, i.e. the aperture angle  $2\alpha = 2\pi$  (see Fig.15(right)) and the number of marigrams engaged in the inversion process is equal to 5 in our study.

### 5. CONCLUSION

We applied an inversion method to the problem of reconstructing the initial water elevation field that generates a tsunami. The numerical simulation of a tsunami source is

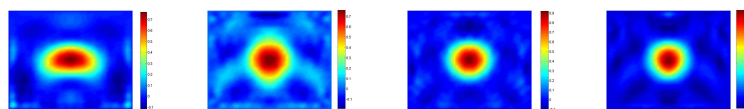


FIG. 16. The recovered functions in *Mod. 9* by the inversion with: 3 receivers;  $\alpha = 0.6\pi$  (left); 5 receivers;  $\alpha = 0.05\pi$  (middle left); 5 receivers;  $\alpha = 0.25\pi$  (middle right); 5 receivers;  $\alpha = \pi$  (right).

one of an important component of the assessment and, thus, mitigation of the effects of the tsunami impact.

The application of  $\mathbf{r}$ -solutions is an effective means of regularization of an ill-posed problem. The number of  $\mathbf{r}$  basic vectors applied appears to be essentially lower than the minimum dimension of the matrix. This, in fact, enables one to avoid the instability of the problem caused by a sharp decrease in singular values of the matrix.

Analysis of the singular spectrum of the matrix obtained allows us to predict a possible quality of the inversion by a given observational system. This result should be kept in mind when designing a tide-gauge network to study a tsunami source.

Since the calculations were really made in the time-spectral domain, we can conclude that for the solution being satisfactory the shortest wavelength should be less than half of the characteristic size of a tsunami source. The number of frequencies used in calculations should not be large; it is sufficient to use about 15 frequencies.

The quality of a solution is improving when the number of receivers increase up to 10-15. The further increase is useless.

We have also shown that a way to improve the inversions with a lesser number of marigrams is to use the wide range of angles of observation. The best range is the entire circle. The results are very satisfactory, since a rough localization of the source enables us to recovery the initial water surface displacement in the source area. This is promises the similar result in more complicated case when the depth of the basin is an arbitrary function of two variables.

#### REFERENCES

- [1] K. Satake, *Inversion of tsunami waveforms for the estimation of a fault heterogeneity: method and numerical experiments*, J. Phys. Earth, **35** (1987), 241–254.
- [2] C. Pires, P.M.A. Miranda, *Tsunami waveform inversion by adjoint methods*, J. Geophys. Res., bf 106 (2001), 19773–19796.
- [3] S. Tinti, A. Piatanesi, and E. Bortolucci, *The finite-element wavepropagator approach and the tsunami inversion problem*, J. Phys. Chem. Earth, **12** (1996), 27–32.
- [4] Donald B. Percival, Donald W. Denbo, Marie C. Eble, Edison Gica, Harold O. Mofjeld, Michael C. Spillane, Liujuan Tang, Vasily V. Titov, *Extraction of tsunami source coefficients via inversion of DART buoy data*, Natural Hazards, **58** (2011), 567–590.
- [5] T. A. Voronina, V. A. Tcheverda, *Reconstruction of tsunami initial form via level oscillation*, Bull. Nov. Comp. Center, Math. Model. in Geoph., **4** (1998), 127–136. Zbl 0955.86001
- [6] T. A. Voronina, *Determination of spatial distribution of oscillation sources by remote measurements on a finite set of points*, Sib. J. Calc. Math., **3** (2004), 203–211. Zbl 1060.86008
- [7] T. Voronina, *Reconstruction of Initial Tsunami Waveforms by a Truncated SVD Method*, J. Inverse and Ill-posed Problems, **19** (2011), 615–629. MR2853115
- [8] Voronina T.A., *Application of  $\mathbf{r}$ -solutions to reconstructing an initial tsunami waveform*, Numerical methods and Programming, **14** (2013), 165–174.
- [9] B. Enquist, A. Majda, *Absorbing boundary conditions for the numerical simulation of waves*, Math. Comp., **139** (1977), 629–654.
- [10] V. M. Kaistrenko, *Inverse problem for reconstruction of tsunami source*, Tsunami Waves. Proc. Sakhalin Compl. Inst., **29** (1972), 82–92.

- [11] V. A. Cheverda, V. I. Kostin, *r-pseudoinverse for compact operator*, Siberian Electronic Mathematical Reports, **7** (2010), 258–282.
- [12] Zuhair Nashed M. *Aspects of generalized inverses in analysis and regularization*, Generalized Inverses and Applications, (1988), 193–244.

TATYANA ALEXANDROVNA VORONINA  
INSTITUTE OF COMPUTATIONAL MATHEMATICS AND MATHEMATICAL GEOPHYSICS SB RAS,  
PR.AC.LAVRENTIEVA, 6,  
630090, NOVOSIBIRSK, RUSSIA  
*E-mail address:* [vta@omzg.sccc.ru](mailto:vta@omzg.sccc.ru)

VLADIMIR ALBERTOVICH TCHEVERDA  
INSTITUTE OF PETROLEUM GEOLOGY AND GEOPHYSICS OF SB RAS,  
PR.KOPTUG, 3,  
630090, NOVOSIBIRSK-90, RUSSIA  
*E-mail address:* [cheverdava@ipgg.nsc.ru](mailto:cheverdava@ipgg.nsc.ru)

VLADISLAV VLADIMIROVICH VORONIN  
NOVOSIBIRSK STATE UNIVERSITY,  
PIROGOVA STR. 2,  
630090, NOVOSIBIRSK-90, RUSSIA  
*E-mail address:* [vladvor48@bk.ru](mailto:vladvor48@bk.ru)